Available online at www.sciencedirect.com

ScienceDirect

IFAC PapersOnline CONFERENCE PAPER ARCHIVE

IFAC PapersOnLine 58-4 (2024) 61–66

Actuator Fault Tolerant Control for a Remotely Operated Vehicle based on Adaptive Extended Kalman Filter

Alessandro Baldini * **Riccardo Felicetti** * **Alessandro Freddi** * **Andrea Monteriù** *

* *Department of Information Engineering, Università Politecnica delle Marche, Via Brecce Bianche, 60131 Ancona, Italy, (e-mail: {a.baldini, r.felicetti, a.freddi, a.monteriu}@univpm.it)*

Abstract: In this paper, we propose a strategy for detecting and isolating actuator faults in an overactuated Remotely Operated Vehicle (ROV) with six degrees of freedom. Fault detection and isolation are based on the Adaptive Extended Kalman Filter (AEKF), which is a recent extension of the well-known Kalman Filter designed for nonlinear dynamics and additive disturbances estimation. The residuals generated by the AEKF act as directional residuals, and fault isolation is performed by calculating the cosine similarity between the residuals and the columns of the control effectiveness matrix. The decision is then used in a simple fault-tolerant control allocation algorithm, without the need to alter the control law. Simulation results show the effectiveness of the estimation method in the presence of thruster failures.

Keywords: Safety of marine systems; Reconfigurable control, sensor and actuator faults.

1. INTRODUCTION

Remotely Operated Vehicles (ROVs) are typically deployed in unstructured and challenging environments, where various unforeseeable events can happen. For instance, the marine currents may act as external disturbances, physical obstacles might obstruct the path of the ROV, and aquatic vegetation can impede the operation of its thrusters (Capocci, 2018). Notably, the presence of aquatic vegetation can lead to a reduction in the effectiveness of the thrusters, causing a Loss Of Effectiveness (LOE). Additionally, issues such as voltage drops and propeller damage can induce partial or total LOE. Thus, the issue of Fault Detection and Isolation (FDI) is highly significant in the context of ROVs.

To perform FDI, the residual must actually be a vector of signals, as FDI is not possible in presence of a scalar residual (Gertler, 2005), at least if no assumptions on the fault magnitude and/or spectral characteristics of the fault signal can be made. For this purpose, two main classes of residuals are investigated in the literature: structured residuals and directional residuals (Chen and Patton, 1999). To perform FDI using structured residuals, the residuals' values are tested in parallel against pre-defined thresholds (Antic et al., 2016). Then, the binary outcome is compared with the structure matrix, that describes if each residual is sensitive to each fault or not. So, the information lies in the dependencies between residuals and faults in a binary way. An alternative approach to achieve FDI involves designing a directional residual vector that aligns with a predefined direction or subspace specific to a given fault. In this case, FDI boils down to identifying the known fault signature direction that best matches the residual vector (Chen et al., 1995; Patton and Chen, 1997) using simple tests based on geometry and generalized likelihood (Hu and Gertler, 2005). Let $r(t)$ be the residual vector. The residual is said directional if $r(t|p_j) = \alpha_j(t)l_j$, where $r(t|p_j)$ is the residual affected by a single fault $p_j(t)$, l_j is a constant vector that identifies the direction of the response in the residual space, and $\alpha_j(t)$ is a scalar that depends on the fault size and dynamics (Chen, 1995; Gertler and Monajemy, 1995). Ideally, the response directions should be orthogonal (or at least linearly independent): this allows for a straightforward isolation, however, it limits the number of faults to that of the system outputs (Gertler, 2005). Observers that produce a residual with directional characteristics are known in the literature as fault (or failure) detection filters, following the seminal work by Beard (1971). Fault detection filters map additive fault vectors to the detection space, spanned by eigenvectors which are colinear in output space. The detection filter design process consists of assigning the eigenstructure of the detection space associated with each fault to achieve the desired directional properties (Park and Rizzoni, 1994) by means of a proper choice of the observer gain (White and Speyer, 1987).

The objective of this paper is to design a fault-tolerant control scheme for an overactuated ROV with 6 degrees of freedom (i.e., position and attitude) using a recent advancement of the well-known Kalman Filter (KF), known as Adaptive Extended Kalman Filter (AEKF), as a directional residual generator. As will become clearer in the remainder of the paper, the conventional KF is not suitable for FDI in such a ROV because the augmented system (i.e., considering the joint state and disturbance) is not uniformly completely controllable regarding the state

10.1016/j.ifacol.2024.07.194

noise. Practically, if a conventional KF is employed in such a model, the estimation of the fault becomes unresponsive because its expected uncertainty converges to zero, making it useless for fault detection. The AEKF has been conceived in Zhang (2018) precisely to overcome this limitation, while Skriver et al. (2019) proposed its extended form for nonlinear systems. In our previous work Baldini et al. (2022a), we focused on how to discern between actuator faults and other external disturbances by means of active fault diagnosis, i.e., by injecting an auxiliary signal in the control inputs. The previous work Baldini et al. (2022b), instead, was devoted to the estimation of the fault magnitude by using a bank of nonlinear observers. However, both works are limited to the system dynamics in the horizontal plane. In the case of overactuated vehicles, like the commercial BlueROV2 Heavy (Wu, 2018), where pitch and roll angles can be commanded independently with redundant actuators, FDI methods based on a bank of observers become more complex, as more possibly faulty actuators require more observers.

The paper is structured as follows. The ROV model is resumed in Section 2. The proposed control scheme, detailed in Section 3, is tolerant with respect to the total failure of a thruster. The FDI strategy, that is based on a directional residual generated by an AEKF, is described in Section 4. Simulation results are presented in Section 5 to show the effectiveness of the fault tolerant control scheme. Finally, conclusions and future works end the paper.

2. MATHEMATICAL MODEL

To develop a model-based FDI algorithm, we first introduce the kinematics and the dynamics of the ROV (Section 2.1 and 2.2, respectively) and its control inputs (Section 2.3), including possible LOE faults affecting the actuators.

2.1 Kinematics

Let us define the state space variables

$$\begin{aligned} \eta &= [\, x \;\; y \;\; z \;\; \phi \;\; \theta \;\; \psi \,]^T \\ \nu &= [\, u \;\; v \;\; w \;\; p \;\; q \;\; r \,]^T \\ \tau &= [\, X \;\; Y \;\; Z \;\; K \;\; M \;\; N \,]^T , \end{aligned} \tag{1}$$

where η denotes the position (x, y, z) and orientation (ϕ, θ, ψ) vector in the inertial earth-fixed frame, ν denotes the linear (u, v, w) and angular (p, q, r) velocities vectors in the body-fixed frame, and τ is the vector of the generalized forces, exerted by the actuators, in the body-fixed frame. We define the principal rotation matrices in the xyz-convention in terms of the Euler angles ϕ, θ, and ψ (pitch, roll, and yaw, respectively) as follows:

$$\begin{aligned} R_z(\psi) &= \begin{bmatrix} \cos(\psi) & -\sin(\psi) & 0 \\ \sin(\psi) & \cos(\psi) & 0 \\ 0 & 0 & 1 \end{bmatrix} \\ R_y(\theta) &= \begin{bmatrix} \cos(\theta) & 0 & \sin(\theta) \\ 0 & 1 & 0 \\ -\sin(\theta) & 0 & \cos(\theta) \end{bmatrix} \\ R_x(\phi) &= \begin{bmatrix} 1 & 0 & 0 \\ 0 & \cos(\phi) & -\sin(\phi) \\ 0 & \sin(\phi) & \cos(\phi) \end{bmatrix} . \end{aligned} \tag{2}$$

Then, the rotation matrix from the body-fixed frame to the earth-fixed frame is:

$$R_b^e(\eta) = R_z(\psi) R_y(\theta) R_x(\phi). \tag{3}$$

The Euler rate vector $\dot{\eta}$ is related to the body-fixed angular velocity vector ν through the transformation matrix

$$T(\eta) = \begin{bmatrix} 1 & \sin(\phi)\tan(\theta) & \cos(\phi)\tan(\theta) \\ 0 & \cos(\phi) & -\sin(\phi) \\ 0 & \sin(\phi)/\cos(\theta) & \cos(\phi)/\cos(\theta) \end{bmatrix} . \tag{4}$$

Thus, the kinematics is modelled by:

$$\dot{\eta} = J(\eta)\nu, \tag{5}$$

where $J(\eta) = \mathrm{diag}\,(R_b^e(\eta),\, T(\eta))$ and $\mathrm{diag}(\cdot)$ returns a square diagonal matrix with the arguments on the main diagonal (block diagonal, if the arguments are matrices).

2.2 Dynamics

The well known generic model for marine vehicles from Fossen (1994) is employed to model the ROV dynamics

$$(M_{rb} + M_a)\dot{\nu} + (C_{rb}(\nu) + C_a(\nu))\nu + D(\nu)\nu + g(\eta) = \tau. \tag{6}$$

Assuming that the origin of the body-fixed frame coincides with the center of gravity, and assuming that the body is symmetric w.r.t. the body axes, the inertia tensor is a diagonal matrix. Hence, the rigid-body inertia matrix boils down to

$$M_{rb} = \mathrm{diag}\,(m,\, m,\, m,\, I_x,\, I_y,\, I_z)\,, \tag{7}$$

where m is the mass of the ROV and I_x, I_y, and I_z represent the inertia along the front, right, and down body-fixed axes respectively, and the rigid-body Coriolis and centripetal matrix is

$$C_{rb}(\nu) = \begin{bmatrix} 0 & 0 & 0 & 0 & mw & -mv \\ 0 & 0 & 0 & -mw & 0 & mu \\ 0 & 0 & 0 & mv & -mu & 0 \\ 0 & mw & -mv & 0 & I_z r & -I_y q \\ -mw & 0 & mu & -I_z r & 0 & I_x p \\ mv & -mu & 0 & I_y q & -I_x p & 0 \end{bmatrix} . \tag{8}$$

In the case of low speed movements and symmetric ROV, the simplified expressions in Fossen (1994) can be adopted

$$M_a = \mathrm{diag}\,(-X_{\dot{u}},\, -Y_{\dot{v}},\, -Z_{\dot{w}},\, -K_{\dot{p}},\, -M_{\dot{q}},\, -N_{\dot{r}}) \tag{9}$$

$$C_a(\nu) = \begin{bmatrix} 0 & 0 & 0 & 0 & -Z_{\dot{w}} w & Y_{\dot{v}} v \\ 0 & 0 & 0 & Z_{\dot{w}} w & 0 & -X_{\dot{u}} u \\ 0 & 0 & 0 & -Y_{\dot{v}} v & X_{\dot{u}} u & 0 \\ 0 & -Z_{\dot{w}} w & Y_{\dot{v}} v & 0 & -N_{\dot{r}} r & M_{\dot{q}} q \\ Z_{\dot{w}} w & 0 & -X_{\dot{u}} u & N_{\dot{r}} r & 0 & -K_{\dot{p}} p \\ -Y_{\dot{v}} v & X_{\dot{u}} u & 0 & -M_{\dot{q}} q & K_{\dot{p}} p & 0 \end{bmatrix} , \tag{10}$$

where M_a is the added mass inertia matrix, $C_a(\nu)$ is the hydrodynamic rigid-body Coriolis and centripetal matrix, and the constant parameters $X_{\dot{u}}$, $Y_{\dot{v}}$, $Z_{\dot{w}}$, $K_{\dot{p}}$, $M_{\dot{q}}$, and $N_{\dot{r}}$ must be experimentally identified. Under the same assumptions, the linear ($D_l(\nu)$) and quadratic ($D_{nl}(\nu)$) hydrodynamic damping matrices can be approximated as follows (Fossen, 1994)

$$\begin{aligned} D(\nu) &= D_l(\nu) + D_{nl}(\nu) \\ D_l(\nu) &= -\mathrm{diag}\,(X_u,\, Y_v,\, Z_w,\, K_p,\, M_q,\, N_r) \\ D_{nl}(\nu) &= -\mathrm{diag}\,\big(\, X_{u|u|}\,|u|\,,\, Y_{v|v|}\,|v|\,,\, Z_{w|w|}\,|w|\,, \\ &\qquad K_{p|p|}\,|p|\,,\, M_{q|q|}\,|q|\,,\, N_{r|r|}\,|r|\,\big)\,, \end{aligned} \tag{11}$$

where X_u, Y_v, Z_w, K_p, M_q, N_r, $X_{u|u|}$, $Y_{v|v|}$, $Z_{w|w|}$, $K_{p|p|}$, $M_{q|q|}$, and $N_{r|r|}$ are constant parameters to be identified as well.

Denoting with b the magnitude of the buoyant force, mg the magnitude of the gravitational force, and x_b, y_b, and z_b the coordinates of the center of buoyancy in the body-fixed frame, under the assumption that the origin of the body-fixed frame coincides with the center of gravity, the restoring forces and moments due to gravity and buoyancy can be modeled as

$$g(\eta) = \begin{bmatrix} -\sin(\theta)(b-mg) \\ \cos(\theta)\sin(\phi)(b-mg) \\ \cos(\phi)\cos(\theta)(b-mg) \\ by_b\cos(\phi)\cos(\theta) - bz_b\cos(\theta)\sin(\phi) \\ -bz_b\sin(\theta) - bx_b\cos(\phi)\cos(\theta) \\ by_b\sin(\theta) + bx_b\cos(\theta)\sin(\phi) \end{bmatrix}. \quad (12)$$

To consider the current-induced forces and moments, it is sufficient to replace ν in (6) with the relative velocity $\nu_r = \nu - \nu_c$, where $\nu_c = [u_c\ v_c\ w_c\ 0\ 0\ 0]$ is the (irrotational) marine current velocity expressed in the body-fixed frame. Thus, the differential equations

$$\dot{\eta} = J(\eta)\nu_r + \nu_c^e \quad (13a)$$

$$\dot{\nu}_r = (M_{rb} + M_a)^{-1} \quad \big(\tau - (C_{rb}(\nu_r) + C_a(\nu_r))\nu_r - D(\nu_r)\nu_r - g(\eta)\big) \quad (13b)$$

represent the nonlinear model of the ROV, where η and ν_r are the state space variables, while $\nu_c^e = J(\eta)\nu_c$ is the marine current velocity expressed in the earth-fixed frame. We assume that η and ν_r are measured and available. Position and attitude are usually calculated by the inertial measurement unit, while the relative velocity can be measured with doppler velocity loggers and acoustic doppler current profilers.

2.3 Control inputs

Let $F_i \in \mathbb{R}$ be the force magnitude required from the ith thruster. Let also $l_i \in \mathbb{R}^3$ be the fixed versor that represents the orientation of the ith thruster in the body-fixed frame, so that $F_i l_i$ is the vector representing the required force of the ith thruster in the body-fixed frame. For the case of the BlueROV 2 Heavy (Wu, 2018), that is equipped with 8 thrusters:

$$\tau = BWF \quad (14a)$$

$$B = [B_1\ \dots\ B_8] = \begin{bmatrix} l_1 & \cdots & l_8 \\ r_1 \times l_1 & \dots & r_8 \times l_8 \end{bmatrix} \quad (14b)$$

$$W = \mathrm{diag}(w_1, \dots, w_8) \quad (14c)$$

$$F = [F_1\ \dots\ F_8]^T, \quad (14d)$$

where $r_i \in \mathbb{R}^3$ represents the position of the ith thruster in the body-fixed frame, $\times$ is the cross product, and $w_i \in \mathbb{R}$ represents the effectiveness of the ith thruster (Baldini et al., 2017). In other words, if w_i decreases from its nominal value $\bar{w}_i = 1$, the ith actuator is affected by a LOE. Each force F_i linearly depends on the commanded thruster speed if low speed movements are assumed (i.e., neglecting the dependence of the force on the relative fluid velocity). Thus, in the remainder, we consider $F \in \mathbb{R}^8$ to be the actual control input variable, without detailing the thruster speed.

3. FAULT TOLERANT CONTROL

Conventional closed-loop control of ROVs makes use a virtual control input $\tau_c \in \mathbb{R}^6$ that is required by the control law to pilot the ROV. Six PIDs calculate the components of τ_c independently, based on the tracking error $\eta_{ref} - \eta \in \mathbb{R}^6$, and $g(\eta)$ is feedforwarded to improve the control performances (Fossen, 1994). The reference comprises the target position and the target orientation, which may be set by the remote operator using a joystick, and the tracking errors are fed to the PIDs. Then, τ_c must be mapped to the actuator commands F, such that $\tau = \tau_c$ holds (at least in nominal actuator conditions). The thrust allocation algorithm that returns such input F is detailed in Section 3.1.

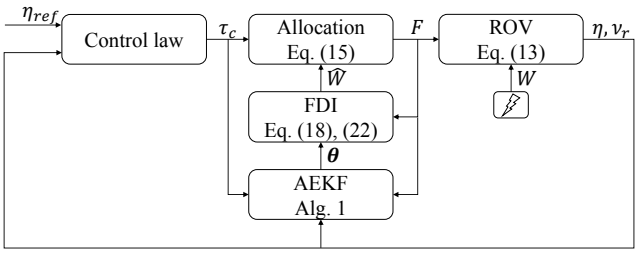

Fig. 1. Fault tolerant control scheme.

In addition to the conventional closed-loop control, we pursue fault tolerance by adding an AEKF-based residual generator, a FDI decision-making algorithm, and the fault tolerant control allocation algorithm detailed in the following. The resulting closed-loop control scheme is illustrated in Fig. 1.

3.1 Fault tolerant control allocation algorithm

A simple thrust allocation algorithm to distribute the effort τ_c among the available thrusters is the pseudoinverse method

$$F = (B\hat{W})^+\tau_c \quad (15a)$$

$$\hat{W} = \mathrm{diag}(\hat{w}_1, \dots, \hat{w}_8), \quad (15b)$$

where $\hat{W}$ is an estimation of W and $(B\hat{W})^+$ is the pseudoinverse of $B\hat{W}$. When no estimations are available, the nominal effectiveness is employed in (15), i.e., $\hat{w}_i = \bar{w}_i = 1$ for $i = 1, \dots, 8$. If a FDI algorithm evaluates the ith thruster to be severely damaged, it is sufficient to set $\hat{w}_i = 0$, hence zeroing the column B_i, i.e., the ith thruster has no effect. As a consequence, if $\hat{w}_i = 0$ is set, the control allocation algorithm simply switches the ith thruster off to minimize the cost function. The reader can refer to Baldini et al. (2018a) for further details.

4. FAULT DETECTION AND ISOLATION

The residual generator is detailed in Section 4.1, while its use for FDI is discussed in Section 4.2 and Section 4.3.

4.1 Residual generation

The model (13)-(14) is discretized with a forward Euler integration, obtaining

$$\boldsymbol{x}(k+1) = \boldsymbol{f}(\boldsymbol{x}(k)) + \boldsymbol{B}(k)\boldsymbol{u}(k) + \boldsymbol{\Phi}(k)\boldsymbol{\theta}(k) + \boldsymbol{w}(k) \quad (16a)$$

$$\boldsymbol{\theta}(k+1) = \boldsymbol{\theta}(k) \quad (16b)$$

$$\boldsymbol{y}(k) = \boldsymbol{C}(k)\boldsymbol{x}(k) + \boldsymbol{v}(k), \quad (16c)$$

where $\boldsymbol{w}(k) \sim (0, \boldsymbol{Q}(k))$ and $\boldsymbol{v}(k) \sim (0, \boldsymbol{R}(k))$ are zero mean white gaussian noises. The proposed fault and disturbance model (16b) simply takes the last sample as the best prediction possible, as no prior information on their time derivative is available. This kind of fault modeling is straightforward yet effective in the case of slowly varying variables (i.e., small time derivatives) and in the case of piecewise-constant variables, where the time derivative is zero almost always (Zhang, 2018). The remaining vectors and matrices are detailed as follows

$$
\begin{aligned}
\boldsymbol{x}(k) &= \begin{bmatrix} \eta(k) \\ \nu_r(k) \end{bmatrix}, \quad \boldsymbol{f}(\boldsymbol{x}(k)) = \begin{bmatrix} \boldsymbol{f}_\eta(\boldsymbol{x}(k)) \\ \boldsymbol{f}_{\nu_r}(\boldsymbol{x}(k)) \end{bmatrix}, \\
\boldsymbol{f}_\eta(\boldsymbol{x}(k)) &= \eta(k) + J(\eta(k))\nu_r(k)T_s, \\
\boldsymbol{f}_{\nu_r}(\boldsymbol{x}(k)) &= \nu_r(k) - (M_{rb} + M_a)^{-1}\big(C_{rb}(\nu_r(k)) + \\
&\quad + C_a(\nu_r(k)) + D(\nu_r(k))\big)\nu_r(k)T_s), \\
\boldsymbol{B}(k) &= \begin{bmatrix} 0_6 \\ (M_{rb} + M_a)^{-1}T_s \end{bmatrix}, \quad \boldsymbol{C}(k) = I_{12}, \\
\boldsymbol{u}(k) &= \tau_c(k) - g(\eta(k)), \\
\boldsymbol{\Phi}(k) &= \begin{bmatrix} I_6 T_s & 0_6 \\ 0_6 & T_s(M_{rb} + M_a)^{-1} \end{bmatrix}, \\
\boldsymbol{\theta}(k) &= \begin{bmatrix} \nu_c^E(k) \\ \boldsymbol{\theta}_F(k) \end{bmatrix}, \quad \boldsymbol{F}(\hat{\boldsymbol{x}}(k)) = \left.\frac{\partial \boldsymbol{f}(\boldsymbol{x}(k))}{\partial \boldsymbol{x}(k)}\right|_{\hat{\boldsymbol{x}}(k)},
\end{aligned}
$$

where I_j represents the square identity matrix with j rows and columns and, analogously, 0_j is the null matrix. Please note that the variable $\boldsymbol{u}(k)$ collects both the virtual control input $\tau(k)$ and the known external disturbances $g(\eta(k))$, while $\boldsymbol{\theta}(k) \in \mathbb{R}^{12}$ groups the marine current $\nu_c^E(k) \in \mathbb{R}^6$ and the actuator fault $\boldsymbol{\theta}_F(k) \in \mathbb{R}^6$.

As anticipated in the introduction, please note that the augmented system (16) is not uniformly completely controllable regarding the state noise, because the disturbances (16b) are not affected by gaussian noise. Hence, given the ROV model in the state space form (16), we employ the AEKF proposed by Skriver et al. (2019) (see Algorithm 1) to get an estimation $\hat{\boldsymbol{\theta}}(k)$ of $\boldsymbol{\theta}(k)$.

4.2 Fault detection

We employ the fault estimation $\hat{\boldsymbol{\theta}}_F(k)$, calculated by the AEKF, as a residual for fault detection. In absence of faults, $\boldsymbol{\theta}_F(k)$ is expected to be zero. However, disturbances and model mismatches affect the estimation, and a proper detection threshold σ_{det} and weighting matrix R_{det} must be defined to avoid false positives. If

$$
r_{det}(k) = \sqrt{\hat{\boldsymbol{\theta}}_F(k)^T R_{det} \hat{\boldsymbol{\theta}}_F(k)} > \sigma_{det}, \tag{17}
$$

then a fault is detected, and fault isolation is performed.

4.3 Fault isolation

After a fault is detected, we are interested in isolating if an actuator is severely damaged. Whenever a thruster is subject to LOE, the nominal generalized force τ_c and the actual one τ can differ significantly. In fact

$$
\begin{aligned}
\tau &= BWF = BW(B\hat{W})^+\tau_c \\
&= B\hat{W}(B\hat{W})^+\tau_c + B(W - \hat{W})(B\hat{W})^+\tau_c \\
&= \tau_c + B(W - \hat{W})F,
\end{aligned} \tag{18}
$$

Algorithm 1 AEKF (Skriver et al., 2019)

Input: State-space representation $\boldsymbol{f}$, $\boldsymbol{B}(k)$, $\boldsymbol{C}(k)$, initial AEKF matrices $\boldsymbol{P}(0|0) = \boldsymbol{P}_0$, $\boldsymbol{S}(0) = \boldsymbol{S}_0$, $\hat{\boldsymbol{x}}(0|0) = \boldsymbol{x}_0$, $\hat{\boldsymbol{\theta}}(0) = \boldsymbol{\theta}_0$ and $\boldsymbol{\Upsilon}(0) = 0$.

$\boldsymbol{P}(k+1|k) \leftarrow \boldsymbol{F}(\hat{\boldsymbol{x}}(k))\boldsymbol{P}(k|k)\boldsymbol{F}^T(\hat{\boldsymbol{x}}(k)) + \boldsymbol{Q}(k)$
$\boldsymbol{\Sigma}(k+1) \leftarrow \boldsymbol{C}(k)\boldsymbol{P}(k+1|k)\boldsymbol{C}^T(k) + \boldsymbol{R}(k)$
$\boldsymbol{K}(k+1) \leftarrow \boldsymbol{P}(k+1|k)\boldsymbol{C}^T(k)\Sigma^{-1}(k+1)$
$\boldsymbol{P}(k+1|k+1) \leftarrow [I_n - \boldsymbol{K}(k+1)\boldsymbol{C}(k)]\,\boldsymbol{P}(k+1|k)$
$\boldsymbol{\Upsilon}(k+1) \leftarrow [I_n - \boldsymbol{K}(k+1)\boldsymbol{C}(k)]\boldsymbol{F}(\hat{\boldsymbol{x}}(k))\boldsymbol{\Upsilon}(k) + [I_n - \boldsymbol{K}(k+1)\boldsymbol{C}(k)]\boldsymbol{\Phi}(k)$
$\boldsymbol{\Omega}(k+1) \leftarrow \boldsymbol{C}(k)\boldsymbol{F}(\hat{\boldsymbol{x}}(k))\boldsymbol{\Upsilon}(k) + \boldsymbol{C}(k)\boldsymbol{\Phi}(k)$
$\boldsymbol{\Lambda}(k+1) \leftarrow \left[\lambda\boldsymbol{\Sigma}(k+1) + \boldsymbol{\Omega}(k+1)\boldsymbol{S}(k)\boldsymbol{\Omega}^T(k+1)\right]^{-1}$
$\boldsymbol{\Gamma}(k+1) \leftarrow \boldsymbol{S}(k)\boldsymbol{\Omega}^T(k+1)\boldsymbol{\Lambda}(k+1)$
$\boldsymbol{S}(k+1) \leftarrow \frac{1}{\lambda}\boldsymbol{S}(k) - \frac{1}{\lambda}\boldsymbol{S}(k)\boldsymbol{\Omega}^T(k+1)\boldsymbol{\Lambda}(k+1)\boldsymbol{\Omega}(k+1)\boldsymbol{S}(k)$
$\tilde{\boldsymbol{y}}(k+1) \leftarrow \boldsymbol{y}(k+1) - \boldsymbol{C}(k)[\boldsymbol{f}(\hat{\boldsymbol{x}}(k)) + \boldsymbol{B}(k)\boldsymbol{u}(k) + \boldsymbol{\Phi}(k)\hat{\boldsymbol{\theta}}(k)]$
$\hat{\boldsymbol{\theta}}(k+1) \leftarrow \hat{\boldsymbol{\theta}}(k) + \boldsymbol{\Gamma}(k+1)\tilde{\boldsymbol{y}}(k+1)$
$\hat{\boldsymbol{x}}(k+1) \leftarrow \boldsymbol{f}(\hat{\boldsymbol{x}}(k)) + \boldsymbol{B}(k)\boldsymbol{u}(k) + \boldsymbol{\Phi}(k)\hat{\boldsymbol{\theta}}(k) + \boldsymbol{K}(k+1)\tilde{\boldsymbol{y}}(k+1) + \boldsymbol{\Upsilon}(k+1)[\hat{\boldsymbol{\theta}}(k+1) - \hat{\boldsymbol{\theta}}(k)]$

Output: State $\hat{\boldsymbol{x}}(k+1)$ and fault $\hat{\boldsymbol{\theta}}(k+1)$ estimations.

and $\tau = \tau_c$, that is perfect matching between the commanded and the actual generalized forces, occurs when $\hat{W} = W$. Consider the control effectiveness (14) and, without loss of generality, the control allocation method in (15). Then , $\tau - \tau_c$ from (18) models an additive fault represents the effects of actuator faults, and we can rewrite

$$
\boldsymbol{\theta}_F(k) = B(W - \hat{W})F = \sum_{i=1}^{8}(w_i - \hat{w}_i)F_i B_i. \tag{19}
$$

Clearly, $\boldsymbol{\theta}_F(k) \in \mathrm{Im}(B)$. Under the assumption that no more than a single actuator fault can occur simultaneously,

$$
\boldsymbol{\theta}_F(k) \in \mathrm{Im}\,(B_i)\,, \tag{20}
$$

where the ith actuator is the one affected by the fault and B_i is the ith column of B defined in (14b). Consequently, the residual $\hat{\boldsymbol{\theta}}_F(k) \in \mathbb{R}^6$ is directional, the direction is a subspace with dimension 1, and its basis is B_i. Please note that each pair (B_i, B_j) is linearly independent whenever $i \neq j$, making the isolation possible.

To isolate the fault, is then sufficient to calculate the direction of $\hat{\boldsymbol{\theta}}_F(k)$. Thus, we check the largest cosine similarity against a threshold σ_{isol}, i.e.,

$$
s_i(k) = \frac{\hat{\boldsymbol{\theta}}_F^T(k) B_i \,\mathrm{sign}(F_i)}{\|\hat{\boldsymbol{\theta}}_F(k)\|\|B_i\|}, \quad i = 1, \ldots, 8 \tag{21a}
$$

$$
s(k) = \max_i s_i(k) > \sigma_{isol}, \tag{21b}
$$

where $\mathrm{sign}(F_i)$ takes into account the current direction of the thrust. In fact, the thrusters are bidirectional and F_i can assume both positive and negative values. So, B_i is the direction in case of forward thrust ($F_i > 0$) and $-B_i$ is the direction in case of reverse thrust ($F_i < 0$), as in (21).

If (17) and (21b) hold, then a severe fault affecting the ith thruster is isolated and the thruster is switched off by setting $w_i = 0$ (see Section 3.1) to prevent further damage. To decrease the number of false positives, a

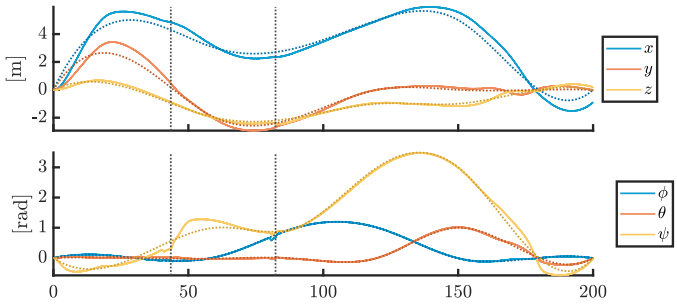

Fig. 2. Position and attitude with reference (dotted line).

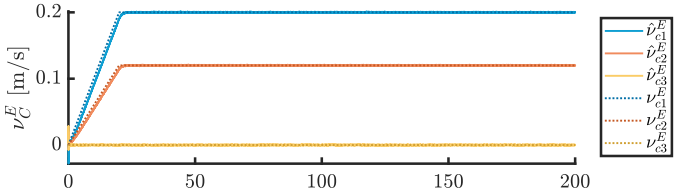

Fig. 3. Marine current (dotted line) and its estimation.

runsum test can be performed, so that the isolation is confirmed if a run of length σ_{run} is generated by the FDI algorithm (i.e., if the outcome is the same for σ_{run} consecutive samples). Finally, please note that (20) holds for any control allocation algorithm, if we assume that input saturation constraints are satisfied, otherwise additional spurious terms may appear. Hence, (20) is expected to hold even more for thruster allocation algorithms that manage input constraints, such as dynamic control allocation (Zaccarian, 2009; Sarkar et al., 2002), quadratic programming solvers (Baldini et al., 2022a), and explicit solutions (Baldini et al., 2018b).

5. SIMULATION RESULTS

We test the fault tolerant control strategy for ROVs on a six degrees of freedom position and attitude tracking problem. The full set of parameters represents a BlueROV 2 Heavy (Wu, 2018) and it is reported in Table 1 for simplicity, together with the control parameters. Two faults are injected: thruster 1 experiences 80% LOE after 40 s and thruster 7 experiences 60% LOE after 80 s. The entire simulation lasts for 200 s. To test the FDI algorithm in a realistic scenario, we enforce a ±5% uniformly distributed uncertainty on every parameter in Table 1, exception made for the mass and the buoyancy. The same uncertainty is set on the nominal thruster effectiveness w_i, for $i = 1, \dots, 8$. The reference is represented in Fig. 2 by a dotted line, while the actual position and attitude are represented by a solid line. Minor attitude errors appear when the fault occurs: the vertical dotted lines highlight the instants when the matrix $\hat{W}$ is updated due to the identification of a failure. The marine current and its estimation by the AEKF are reported in Fig. 3. Please note the estimation is reliable even when the current is not constant. The fault estimation $\hat{\boldsymbol{\theta}}_F(k)$ from the AEKF is reported in Fig. 4. The estimation lumps slowly varying unknown disturbances due to parametric uncertainty and abrupt faults. The black solid line represents the detection residual r_{det}, that reaches the threshold (horizontal dotted line) after 40 s and after 80 s, approximately. In Fig. 5, we report the cosine similarity (21) for each time instant. However, please note

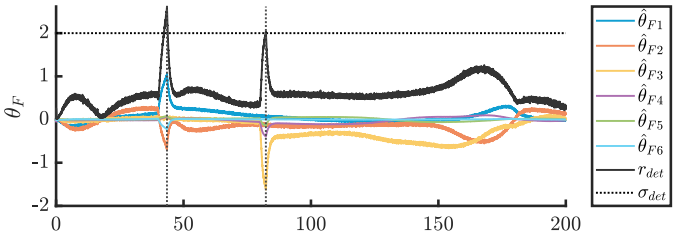

Fig. 4. Fault detection: estimation, residual, threshold.

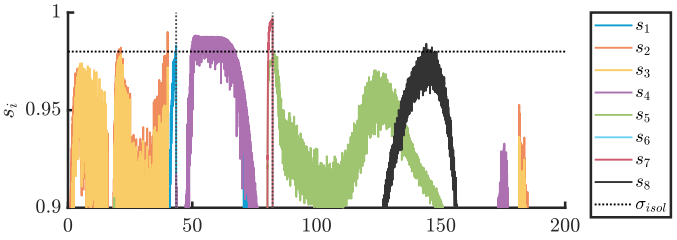

Fig. 5. Fault isolation: cosine similarities and threshold.

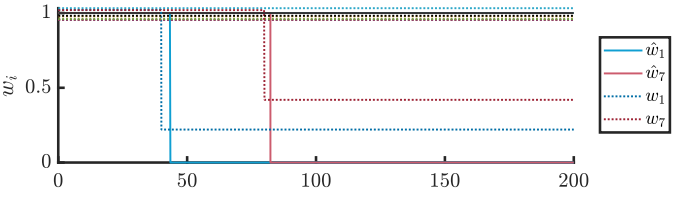

Fig. 6. Actuator effectiveness and failure estimation.

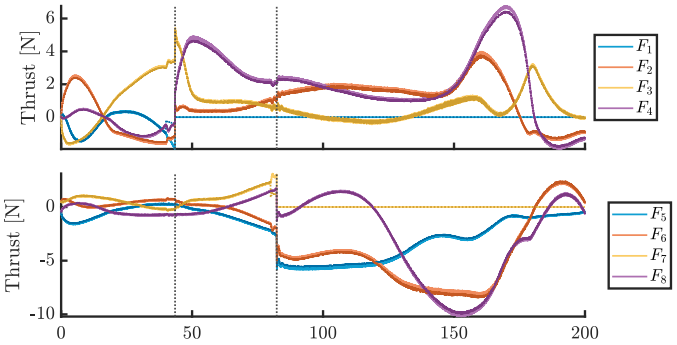

Fig. 7. Commanded thrust and actual thrust (N).

that it is sufficient to calculate it only when a fault is detected, i.e., when (17) holds true. The tests indicate severe damage for thrusters 1 and 7, respectively, as s_1 and s_7 overcome the threshold σ_{isol}, respectively. The dashed lines in Fig. 6 report the actual effectiveness w_i of each thrusters. Note that a ±5% uniformly distributed uncertainty is applied to simulate actuator model mismatch. As stated in Section 3.1, as soon as the FDI rule in (21) highlights the presence of a severe fault on the actuators 1 and 7, $\hat{w}_1$ and $\hat{w}_7$ are set to zero to switch off such thrusters and compensate the failure. The remaining w_i are kept to the nominal value $\bar{w}_i = 1$, as no better estimation is available. The forces required to the actuators are reported in Fig. 7, where $F_1, \dots, F_4$ refer to the horizontal thrusters and $F_5, \dots, F_8$ to the vertical ones. The solid line is the commanded force, while the dotted line is the actual force, affected by both severe LOE and actuator model mismatch. When the fault occurs, the actual force of the thruster is significantly smaller than the commanded one,

Table 1. Model parameters and control parameters.

m	b	x_b, y_b	z_b	I_x, I_y, I_z	$X_{\dot{u}}$	$Y_{\dot{v}}$	$Z_{\dot{w}}$	$K_{\dot{p}}$, $M_{\dot{q}}$, $N_{\dot{r}}$	X_u	Y_v	Z_w
11.5	114.777	0	−0.02	0.16	−5.5	−12.7	−14.57	−0.12	−4.03	−6.22	−5.18

K_p, M_q, N_r	$X_{u\|u\|}$	$Y_{v\|v\|}$	$Z_{w\|w\|}$	$K_{p\|p\|}$, $M_{q\|q\|}$, $N_{r\|r\|}$
−0.07	−18.18	−21.66	−36.99	−1.55

$\{K_i, K_d, K_p, N\}_{PID_x, PID_y}$	$\{K_i, K_d, K_p, N\}_{PID_z}$	$\{K_i, K_d, K_p, N\}_{PID_\phi}$	$\{K_i, K_d, K_p, N\}_{PID_\theta}$	$\{K_i, K_d, K_p, N\}_{PID_\psi}$
$\{3\ 0.2\ 5\ 5\}$	$\{3\ 0.2\ 0.5\ 5\}$	$\{4\ 3\ 0.5\ 5\}$	$\{4\ 3\ 1\ 5\}$	$\{2\ 0.1\ 0.5\ 5\}$

R_{det}	σ_{det}	σ_{isol}	σ_{run}	λ	$\boldsymbol{P}_0$	$\boldsymbol{S}_0$	$\boldsymbol{\theta}_0$	$\hat{\boldsymbol{x}}_0$	$\boldsymbol{R}(k)$	$\boldsymbol{Q}(k)$
$\mathrm{diag}\left(4,\ 4,\ 1,\ 8,\ 8,\ 8\right)$	2	0.98	10	0.999	I_{12}	I_{12}	0	0	$10^{-3}\mathrm{diag}\left(1.6I_3,\ 1.4I_3,\ 3.1I_3,\ 2.8I_3\right)$	$I_{12}10^{-6}$

triggering the FDI. As soon as the thruster is switched off, the effort is redistributed among the remaining actuators.

6. CONCLUSIONS AND FUTURE WORKS

In this paper, we have shown a fault tolerant control strategy applied to tracking control for a BlueROV 2 Heavy ROV with six degrees of freedom. The scheme relies on measuring the entire state space and provides a filtered estimation, through the AEKF, of the state, the actuator fault, and the marine current. Please note that the relative velocity must be measured to perform the fault and current estimation. If only the absolute velocity can be measured, then the proposed scheme can work only in absence of marine current, unless some external estimation of the marine current is provided. In this case, the AEKF can be designed on the dynamics equations only, i.e., neglecting the kinematics, with a substantial decrease in computational effort. However, the estimation of the marine current is not possible in this case. In our future works we are investigating the introduction of active fault diagnosis to discern different faults and the practical case of multi-rate measurements.

REFERENCES

Antic, S., Djurovic, Z., and Kvascev, G. (2016). Application of structured and directional residuals for fault detection and isolation on permanent-magnet dc motor with amplifier. *Quality and Reliability Engineering International*, 32(7), 2601–2621.

Baldini, A., Ciabattoni, L., Felicetti, R., Ferracuti, F., Monteriù, A., Fasano, A., and Freddi, A. (2017). Active fault tolerant control of remotely operated vehicles via control effort redistribution. In *Proceedings of the ASME Design Engineering Technical Conference*, volume 9. doi:10.1115/DETC2017-67760.

Baldini, A., Ciabattoni, L., Felicetti, R., Ferracuti, F., Freddi, A., and Monteriù, A. (2018a). Dynamic surface fault tolerant control for underwater remotely operated vehicles. *ISA Transactions*, 78, 10–20.

Baldini, A., Fasano, A., Felicetti, R., Freddi, A., Longhi, S., and Monteriù, A. (2018b). A constrained thrust allocation algorithm for remotely operated vehicles. *IFAC-PapersOnLine*, 51(29), 250–255.

Baldini, A., Felicetti, R., Freddi, A., Longhi, S., and Monteriù, A. (2022a). Actuator fault tolerant control via active fault diagnosis for a remotely operated vehicle. *IFAC-PapersOnLine*, 55(6), 310–316.

Baldini, A., Felicetti, R., Freddi, A., Longhi, S., and Monteriù, A. (2022b). Fault tolerant control for remotely operated vehicles with thruster faults using nonlinear disturbance observers. *IFAC-PapersOnLine*, 55(31), 275–280.

Beard, R.V. (1971). *Failure accomodation in linear systems through self-reorganization.* Ph.D. thesis, Massachusetts Institute of Technology.

Chen, J., Patton, R., and Zhang, H. (1995). Design of robust structured and directional residuals for fault isolation via unknown input observers. In *European Control Conference*, 348–353.

Chen, J. (1995). *Robust residual generation for model-based fault diagnosis of dynamic systems.* Ph.D. thesis, University of York.

Chen, J. and Patton, R.J. (1999). *Robust Model-Based Fault Diagnosis for Dynamic Systems.* Springer US, Boston, MA.

Fossen, T. (1994). *Guidance and Control of Ocean Vehicles.* Wiley.

Gertler, J. (2005). Residual generation from principal component models for fault diagnosis in linear systems-part i: Review of static systems. In *Proceedings of the 2005 IEEE International Symposium on, Mediterrean Conference on Control and Automation Intelligent Control, 2005.*, 628–633. IEEE.

Gertler, J.J. and Monajemy, R. (1995). Generating directional residuals with dynamic parity relations. *Automatica*, 31(4), 627–635.

Hu, Y. and Gertler, J. (2005). Performance analysis for directional residual based fault isolation. *IFAC Proceedings Volumes*, 38(1), 173–178. 16th IFAC World Congress.

Park, J. and Rizzoni, G. (1994). An eigenstructure assignment algorithm for the design of fault detection filters. *IEEE Trans. on Automatic Control*, 39(7), 1521–1524.

Patton, R.J. and Chen, J. (1997). Observer-based fault detection and isolation: Robustness and applications. *Control Engineering Practice*, 5(5), 671–682.

Sarkar, N., Podder, T., and Antonelli, G. (2002). Fault-accommodating thruster force allocation of an auv considering thruster redundancy and saturation. *IEEE Trans. on Robotics and Automation*, 18(2), 223–233.

Skriver, M., Helck, J., and Hasan, A. (2019). Adaptive extended kalman filter for actuator fault diagnosis. In *2019 4th International Conference on System Reliability and Safety (ICSRS)*, 339–344. IEEE.

White, J. and Speyer, J. (1987). Detection filter design: Spectral theory and algorithms. *IEEE Transactions on Automatic Control*, 32(7), 593–603.

Wu, C.J. (2018). *6-dof modelling and control of a remotely operated vehicle.* Ph.D. thesis, Flinders University, College of Science and Engineering.

Zaccarian, L. (2009). Dynamic allocation for input redundant control systems. *Automatica*, 45(6), 1431–1438.

Zhang, Q. (2018). Adaptive kalman filter for actuator fault diagnosis. *Automatica*, 93, 333–342.